Vol 14 No 7, July 2005
1009-1963/2005/14(07)/1407-06

Chinese Physics

© 2005 Chin. Phys. Soc.
and IOP Publishing Ltd

Optimal injection scheme for electron acceleration by a tightly focused laser beam*

Chen Min(陈 民), Sheng Zheng-Ming(盛政明), and Zhang Jie (张 杰)†

Laboratory of Optical Physics, Institute of Physics, Chinese Academy of Sciences, Beijing 100080, *China*

(Received 6 December 2004; revised manuscript received 10 January 2005)

Electron dynamics and energy gain in a tightly focused laser beam in vacuum are investigated by numerical simulations. There exist two acceleration mechanisms, i.e. acceleration by the longitudinal field or by the transverse field, which corresponds to two different trajectories. The relationship between the energy gain and the injection parameters of electrons, including the injection angle and momentum, is shown. For given laser parameters, the optimum injection parameters can be obtained.

Keywords: laser acceleration, particle acceleration, plasmas, energy gain
PACC: 5240D, 5275D, 4260, 2910

With the rapid advances in laser technology,[1−3] laser acceleration of charged particles becomes one of the frontiers of research. Many acceleration schemes have been proposed. Some of them are related to laser–plasma interaction, such as the plasma beatwave accelerator (PBWA),[4,5] plasma wakefield accelerator (PWFA),[6,7] laser wakefield accelerator (LWFA),[8] betatron-resonance acceleration in the self-focusing channel of a laser pulse[9] and stochastic heating by counter-propagating laser pulses in plasma.[10] At the same time, vacuum laser acceleration scheme has also been studied extensively,[11−18] one of which is the transverse ponderomotive scattering,[11] the other is the longitudinal ponderomotive acceleration.[12] It has also been demonstrated, by numerical simulations, that a single electron injected at a certain angle to the axis of a laser beam, may be captured and accelerated up to GeV energies.[17] Some studies propose that the reason is the phase slippage of the electron in the wave field remains extremely slow which is called the capture and acceleration scheme (CAS).[16−19]

In this paper, we attack the problem of the last vacuum laser acceleration process. It is found that electrons which are trapped by the wave field can be accelerated by both transverse and longitudinal fields, depending upon the injection angles. Optimum injection angles and injection momentum for the maximum energy gain from both fields are found. Furthermore, there exists another acceleration trajectory which is different from the CAS, whose energy gain is not as effective as CAS.

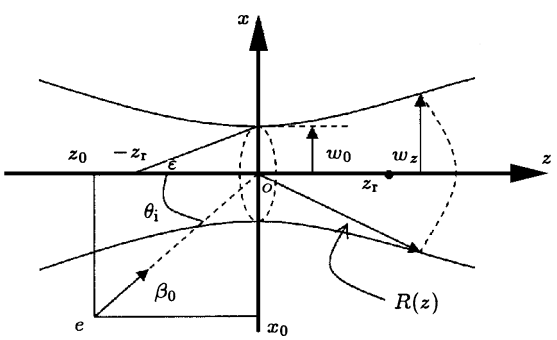


Fig.1. The beam-particle interaction geometry.

The interaction geometry in the x-z plane is shown in Fig.1, where a laser beam is polarized in x-direction and propagates along z-axis. A test electron is injected from the position (x_0, y_0) at an angle θ_i to the z axis with a momentum $\beta_0\gamma_0$ normalized by mc, where $\gamma_0 = 1/\sqrt{1-\beta_0^2}$. Up to now, most of the extremely high intensity laser fields are obtained by focusing laser beams to extremely small spatial dimensions, typically a few microns. This requires a

*Project partially supported by the National Natural Science Foundation of China (Grant Nos 10335020, 10105014 and 10390160), the National High-Tech ICF program, and the National Key Basic Research Special Foundation (Grant No G1999075200).
†Corresponding author, E-mail: jzhang@aphy.iphy.ac.cn

good knowledge of the laser's electric and magnetic fields near the beam focus. A small deviation from the exact fields can lead to completely different particle motion in the high fields. We use a field including the fifth-order terms in terms of the diffraction angle ε, as defined later. The fields are described as follows:[15,20,21]

$$E_x = E\left\{ S_0 + \varepsilon^2\left[\xi^2 S_2 - \frac{\rho^4 S_3}{4}\right] + \varepsilon^4\left[\frac{S_2}{8} - \frac{\rho^2 S_3}{4} - \frac{\rho^2(\rho^2-16\xi^2)S_4}{16} - \frac{\rho^4(\rho^2+2\xi^2)S_5}{8} + \frac{\rho^8 S_6}{32}\right]\right\}, \quad (1)$$

$$E_y = E\xi\zeta\left\{\varepsilon^2 S_2 + \varepsilon^4\left[\rho^2 S_4 - \frac{\rho^4 S_5}{4}\right]\right\}, \quad (2)$$

$$E_z = E\xi\left\{\varepsilon C_1 + \varepsilon^3\left[-\frac{C_2}{2} + \rho^2 C_3 - \frac{\rho^4 C_4}{4}\right] + \varepsilon^5\left[-\frac{3C_3}{8} - \frac{3\rho^2 C_4}{8} + \frac{17\rho^4 C_5}{8} - \frac{3\rho^6 C_6}{8} + \frac{\rho^8 C_7}{32}\right]\right\}, \quad (3)$$

$$B_x = 0, \quad (4)$$

$$B_y = E\left\{ S_0 + \varepsilon^2\left[\frac{\rho^2 S_2}{2} - \frac{\rho^4 S_3}{4}\right] + \varepsilon^4\left[-\frac{S_2}{8} + \frac{\rho^2 S_3}{4} + \frac{5\rho^4 S_4}{16} - \frac{\rho^6 S_5}{4} + \frac{\rho^8 S_6}{32}\right]\right\}, \quad (5)$$

$$B_z = E\zeta\left\{\varepsilon C_1 + \varepsilon^3\left[\frac{C_2}{2} + \frac{\rho^2 C_3}{2} - \frac{\rho^4 C_4}{4}\right] + \varepsilon^5\left[\frac{3C_3}{8} + \frac{3\rho^2 C_4}{8} + \frac{3\rho^4 C_5}{16} - \frac{\rho^6 C_6}{4} + \frac{\rho^8 C_7}{32}\right]\right\}, \quad (6)$$

where $\xi = x/w_0$, $\zeta = y/w_0$, $r^2 = x^2 + y^2$, $\rho = r/w_0$, and $E = E_0\dfrac{w_0}{w}\exp\left[-\dfrac{r^2}{w^2}\right]$ for a beam radius w_0 at the focus, the radius away from the focus $w(z) = w_0\sqrt{1+(z/z_\mathrm{r})^2}$, the Rayleigh length $z_\mathrm{r} = kw_0^2/2$, $k = 2\pi/\lambda$, and the diffraction angle $\varepsilon = w_0/z_\mathrm{r}$. Also there are

$$S_n = \left(\frac{w_0}{w}\right)^n \sin\left(\psi + n\psi_\mathrm{G}\right), \quad n = 0, 1, 2, \ldots, \quad (7)$$

$$C_n = \left(\frac{w_0}{w}\right)^n \cos\left(\psi + n\psi_\mathrm{G}\right), \quad (8)$$

where $\psi = \psi_0 + \psi_\mathrm{p} - \psi_\mathrm{R} + \psi_\mathrm{G}$, ψ_0 is a constant phase, $\psi_\mathrm{p} = \eta = \omega t - kz$ is the plane wave phase, $\psi_\mathrm{G} = \tan^{-1}(z/z_\mathrm{r})$ is the Guoy phase associated with the fact that a Gaussian beam undergoes a total phase change of π as z changes from $-\infty$ to $+\infty$, $\psi_\mathrm{R} = kr^2/(2R)$ is the phase associated with the curvature of the wave fronts, $R(z) = z + z_\mathrm{r}^2/z$ is the radius of curvature of a wave front intersecting the beam axis at the coordinate z. The fields given above satisfy the Maxwell equations in vacuum up to the order ε^6. If the boundary of the beam is defined as where the field amplitude is 1/e of the amplitude on axis, then the solid curves shown in the x–z plane in Fig.1 are defined by $x = \pm w(z)$.

As usually done, we discuss the dynamics of a test electron with mass m and charge $-e$ by numerically integrating the equation of motion:

$$\frac{\mathrm{d}\boldsymbol{r}}{\mathrm{d}t} = \frac{\boldsymbol{p}}{\gamma}, \quad \frac{\mathrm{d}\boldsymbol{p}}{\mathrm{d}t} = -2\pi[\boldsymbol{E} + \boldsymbol{\beta}\times\boldsymbol{B}], \quad (9)$$

where the Lorentz factor $\gamma = \left(1-\boldsymbol{\beta}^2\right)^{-1/2}$, $\boldsymbol{\beta}$ is the electron's velocity normalized by the speed c of light in vacuum and $\boldsymbol{p} = \gamma\boldsymbol{\beta}$ is the momentum normalized by mc, the spatial coordinates $\boldsymbol{r}$ and the time t are normalized by wavelength λ and laser period T, respectively. The electric field $\boldsymbol{E}$ and magnetic field $\boldsymbol{B}$ are all normalized by $mc\omega/e$. We use the fourth-order Runge–Kutta method with changing time-step to keep a high accuracy. The minimal time step is 0.001T with the laser oscillation period T, which is sufficient for the fields considered in this paper. In our simulations, the beam parameter is fixed, where the focus radius $w_0 = 10\mu$m, the laser wavelength is 1μm, the peak intensity is 1.24×10^{21}W/cm^2, corresponding to a power of about 2×10^{15}W. By using the well-known formula $I_0\lambda^2 \approx 1.375\times10^{18}a^2$, the normalized field amplitude $a = eE_0/mc\omega = 30$. Wang *et al*[19] pointed out, that the fraction of electrons captured by laser can reach more than 20% when the incident cross-section of electrons has the size comparable with radius of laser beam at the focus. Without losing generality, in our following simulation the test electron is injected from the same position at $x_0 = -40\lambda$, $z_0 = -320\lambda$ which is reasonable because the fields near this position with our parameters are small and it can only change the injection parameters slightly. Certainly in real experiments the injection position is much farther away. A typical simulation runs up to a time period about 6000T, which is usually long enough to see the final energy and final trajectory inferred from our sim-

ulations at longer time.

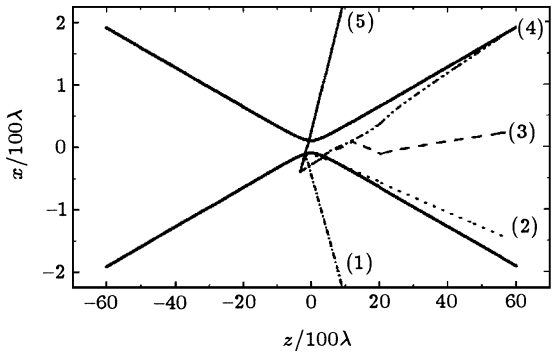


Fig.2. Five typical electron trajectories. The thick solid line shows the boundaries of the laser beam profile defined as $w(z) = w_0\sqrt{1+(z/z_r)^2}$. The injection parameters $(\theta_i, \gamma_0\beta_0)$ for the five trajectories from (1) to (5) are (10°, 20), (10°, 10), (2°, 200), (2°, 300), and (12°, 120), respectively.

Figure 2 shows five typical trajectories of the test electron. The injection parameters $(\theta_i, \gamma_0\beta_0)$ for the five trajectories from (1) to (5) are (10°, 20), (10°, 10), (2°, 200), (2°, 300), and (12°, 120), respectively. From bottom to top, they are identified as a reflection trajectory (1), a lower-boundary trajectory (2), a forward-moving trajectory (3), an upper-boundary trajectory (4) and a crossing trajectory (5), respectively. As seen from Fig.2, the electron trajectory depends strongly on its initial injection parameters, i.e. the injection angle and injection momentum. For the purpose of the particle acceleration, one cares most the energy gain. Of the five trajectories only two give effective acceleration. One is the low-boundary trajectory (2).[16–18] The other is the forward-moving trajectory (3), which is around the axis along which the laser beam propagates. We find the former is better for electron acceleration than the latter. The energy gains ($\Delta\gamma = \gamma - \gamma_0$) corresponding to trajectories (1) to (5) in Fig.2 are about –9.4, 884.3, 261.7, –15.9, 0.1, respectively. Electrons with trajectories like (1) and (5) almost do not change their energies after the interaction with the laser beam, those with trajectories like (4) are decelerated, and the electrons with trajectories like (2) and (3) can be accelerated.

In order to find the optimum injection angle of the test electron, we fix the parameters of the laser beam and the injection position and the injection momentum of the electron, and change the injection angle. As Fig.3 shows, when the injection momentum $\gamma_0\beta_0$ is between 10.0 and 20.0, there exist some injection angles at which the energy gain is high. The two energy–gain peaks in Fig.3(a) imply that there may be two different acceleration mechanisms, even though the corresponding trajectories are all similar to the lower-boundary trajectory (2) as shown in Fig.2 and later in Fig.4. The valley between the peaks corresponds to a reflection trajectory (1). Simulations also show that, when the injection momentum becomes larger, the energy gain peaks usually appear at smaller injection angles.

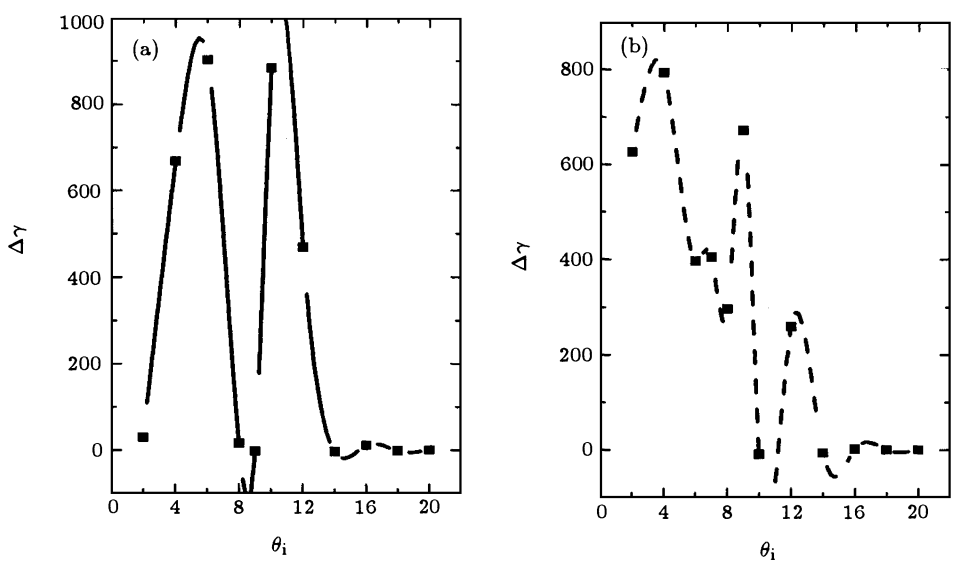


Fig.3. Energy gain $\Delta\gamma$ vs the injection angle θ_i. for the normalized injection momentum $\gamma_0\beta_0 = 10$ (a) and 20 (b).

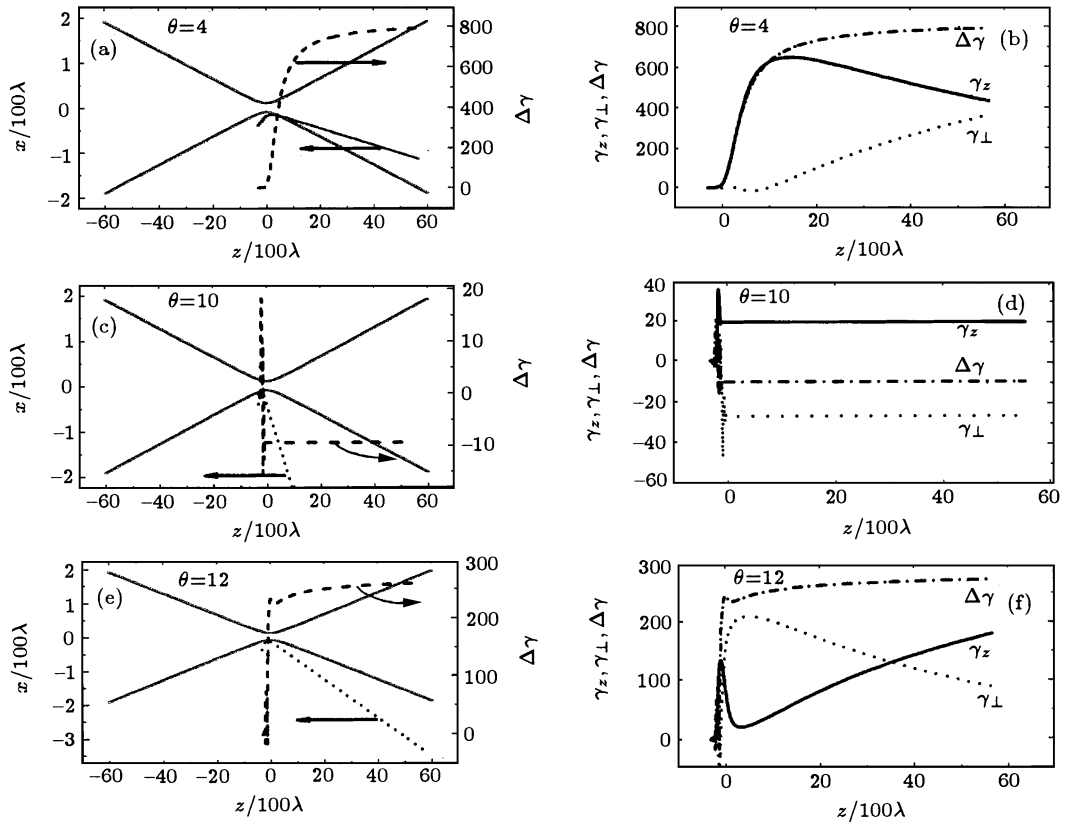


Fig.4. Electron trajectory and the energy gain vs the longitudinal coordinate z for injection parameters $(\theta_i, \gamma_0\beta_0) = (4°, 20)$ (a), $(10°, 20)$ (c), and $(12°, 20)$ (d). Energy gains due to the transverse and longitudinal fields for the above injection parameters are given in (b), (d), and (f), respectively.

In Figs.4(a), 4(c), and 4(e), we show the electron trajectories corresponding to the two energy–gain peaks and the energy valley for the fixed injection momentum as in Fig.3. As stated above, the trajectories for energy-gain peaks are close to the lower-boundary, one above and the other below it. The electrons gain energy mainly near the laser focus within a few Rayleigh lengths, beyond which the electron energy changes very little. As shown by Eqs.(1)–(3), the laser fields contain two transverse components and a longitudinal component. As a result, in principle, electrons can gain energy from both the transverse field and longitudinal field. However, from the electron trajectories, it is difficult to find the acceleration mechanisms. On the other hand, from Eq.(9), one finds that the electron gain can be written as[10]

$$\begin{aligned} \mathrm{d}\gamma/\mathrm{d}t =& -2\pi(v_x E_x + v_y E_y + v_z E_z) \\ \equiv& \mathrm{d}\gamma_\perp/\mathrm{d}t + \mathrm{d}\gamma_z/\mathrm{d}t, \end{aligned} \tag{10}$$

where $\gamma_\perp$ and γ_z represents the energy gain from the transverse and longitudinal fields, respectively. By calculating $\gamma_\perp$ and γ_z for each trajectory, one can find the real acceleration mechanisms. Figures 4(b), 4(d), and 4(f) illustrate the $\gamma_\perp$ and γ_z as a function of the longitudinal coordinate for corresponding trajectories shown in Figs.4(a), 4(c), and 4(e), respectively. Obviously, at the beginning the energy gain for trajectory in Fig.4(a) is dominantly due to γ_z, i.e., the longitudinal field. Later on, γ_z decreases slowly while $\gamma_\perp$ increases slowly in a quite long distance until the electron is far from the focus, typically 20000 wavelengths. As a sum, the total energy remains almost a constant. On the contrary, the energy gain for trajectory in Fig.4(e) is dominantly due to $\gamma_\perp$, i.e., the transverse field at the beginning. Later on, $\gamma_\perp$ decreases while γ_z increases. Also, the total energy remains almost a constant. Generally, the energy gain by the transverse electric field is dominant when the injection angle is relatively large. At the same time, the resulting ejection angle is also large. When the injection angle is small and the turning point of the electron, where the transverse velocity (along x-direction) is zero, is behind the laser focus, the energy gain is mostly due to the longitudinal field.

As stated above for Figs.4(b) and 4(f), the energy gains from the transverse and longitudinal fields cancel each other for electrons moving far away from the laser focus. This means $E_z \mathrm{d}z \approx -E_x \mathrm{d}x$ or

$E_z/E_x \approx -\beta_x/\beta_z$. One can prove this as follows. For $z \gg z_r$, we reserve the first order of the electric fields and obtain

$$\frac{E_z}{E_x} = \frac{\varepsilon E \xi C_1}{E S_0} = \frac{x\cos(\psi+\psi_G)}{\sqrt{z^2+z_r^2}\sin(\psi)} \approx -\frac{x}{\sqrt{z^2+z_r^2}} \approx -\frac{x}{z} \approx -\frac{\beta_x}{\beta_z}, \qquad (11)$$

where we have substituted $\psi_G = \pi/2$ for $z \gg z_r$. Therefore it is the field structure that causes the cancelling of the energy gains from the transverse and longitudinal fields.

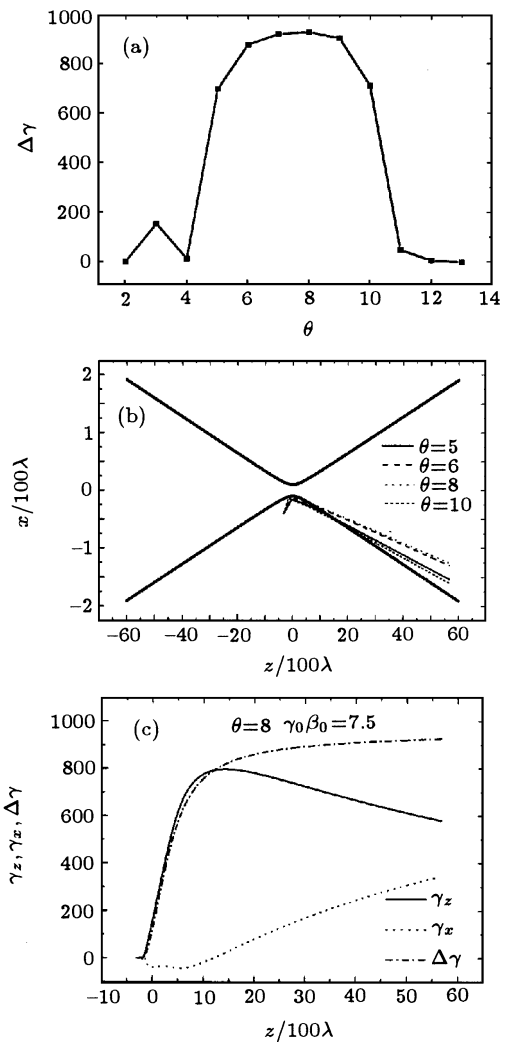


Fig.5. (a) Energy gain as a function of the injection angle for an injection momentum of 7.5 mc; (b) Electron trajectories for injection angles of 5°, 6°, 8°, 10°; (c) Energy gains due to the longitudinal and transverse fields for the injection angle of 8° and injection momentum of 7.5 mc.

When the injection momentum is reduced from these for Fig.3, so that it is not high enough to approach the high field region inside the focus, the electron will not be reflected away with a large scattering angle. In this case, if one changes the injection angle, there is only one peak for energy gain, as shown in Fig.5(a), for example. There is no region for reflection trajectory between energy–gain peaks as shown in Fig.3. Around the angles for the energy–gain peak, all the electron trajectories are slightly above the lower-boundary as shown in Fig.5(b). In this case, the energy gain is predominantly due to the longitudinal field at the beginning as shown in Fig.5(c). Later on, the transverse field also contributes to the energy gain while that due to the longitudinal field decreases.

In another series of simulations, we fix the injection angle but change the injection momentum. As shown in Fig.6, there exits an optimum injection momentum for the largest energy gain. If the injection momentum is too large, the energy gain tends to be zero or even negative. Usually the electron is reflected away or goes directly cross the laser beam in this case. Both of these two trajectories are not suitable for the acceleration. For fixed laser parameters as above and given injection momentum, there is an optimum injection angle for the highest energy gain. Figure 7 illustrates the highest energy gain and the optimum injection angle as a function of injection momentum, i.e. $\Delta\gamma_{max}(\theta_{opt}, \gamma_0\beta_0)$ and $\theta_{opt}(\gamma_0\beta_0)$. It shows that the electrons can get considerable energy as long as the injection parameters are optimized. In our simulation, the maximum energy gain is 450MeV for our laser beam parameters given at the beginning. Larger injection momentum does not mean larger energy gain. In addition, Fig.7 also shows that the larger the injection momentum, the smaller the optimum injection angle.

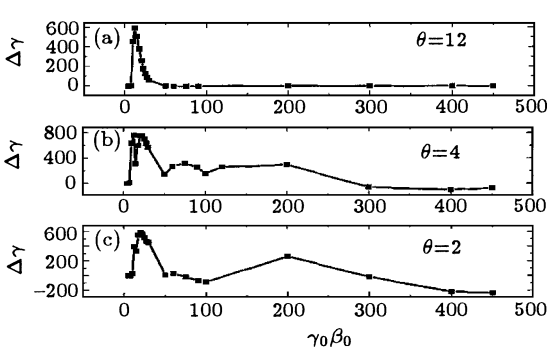


Fig.6. Energy gain vs injection momentum for injection angles of 12° (a), 4° (b), and 2° (c).

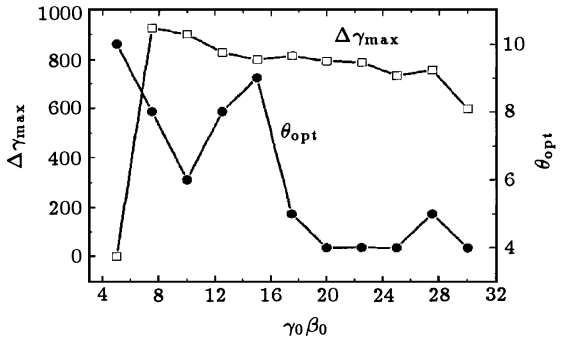


Fig.7. Maximum energy gain as a function of injection momentum at the optimum injection angle. The optimum injection angles are also shown as a function of the injection momentum.

In previous examples, electrons are injected in the polarization plane (xz-plane in our geometric configuration). If electrons are injected in the yz-plane, simulations show that they are more easily scattered out of the high-field regions. As a result, acceleration is usually not as effective as in the polarization plane.

In passing, we mention that for electron trajectories along the propagation axis as shown in Fig.2 for trajectory (3), electron energy gain is mainly due to the longitudinal field. Usually its energy gain is not as effective as for the trajectory (2). Also this trajectory usually occurs when the injection energy is much larger than the ponderomotive potential peak of the laser beam, i.e. $\gamma_0 \gg \sqrt{1+a_0^2/2}$. Further study is still underway.

In summary, it is illustrated that there are typically five different trajectories for electron motion in a tightly focused laser beam, two of which give high energy gains for injection electrons. It shows that there are two different mechanisms for effective electron acceleration, one dominantly from the longitudinal field and another from the transverse field, corresponding to two slightly different trajectories in CAS. The relationship between the energy gain and the injection angle and injection momentum is also shown. Generally, electrons with high injection momenta are injected preferably at a small angle to have a relatively large energy gain. By using appropriate injection parameters, electrons can gain hundreds of MeV of energy from a Petawatt laser beam. With such a laser beam, the injection energy of electrons should preferably be larger than 3.5MeV but less than 15MeV.

References

[1] Strickland D and Mourou G 1985 *Opt. Commun.* **264** 219

[2] Maine P *et al* 1988 *IEEE J. Quantum Electron.* **QE-24** 298

[3] Yang H *et al* 2001 *Acta Phys. Sin.* **50** 1930 (in Chinese)

[4] Tajima T and Dawson J M 1979 *Phys. Rev. Lett.* **43** 267

[5] Kitagawa Y, Matsumoto T, Minamihata T *et al* 1992 *Phys. Rev. Lett.* **68** 48

[6] Rosenzweig J B, Cline D B, Cole B, Figueroa H *et al* 1988 *Phys. Rev. Lett.* **61** 98

[7] Rosenzweig J B, Schoessow P, Cole B *et al* 1989 *Phys. Rev.* A **39** 1586

[8] Chiou T C, Katsouleas T, Decker C, Mori W B, Wurtele J S, Shvets G and Su J J 1995 *Phys. Plasmas* **2** 310

[9] Pukhov A, Sheng Z M and Meyer-ter-Vehn J 1999 *Phys. Plasmas* **6** 2847

[10] Sheng Z M, Mima K, Sentoku Y *et al* 2002 *Phys. Rev. Lett.* **88** 055004
Sheng Z M, Mima K, Zhang J and Meyer-ter-Vehn J 2004 *Phys. Rev.* E **69** 016407

[11] Hartemann F V, Fochs S N, Le Sage G P and Luhamann N C *et al* 1995 *Phys. Rew.* E **51** 4833

[12] He F, Yu W, Lu P X *et al* 2004 *Acta Phys. Sin.* **53** 165 (in Chinese)

[13] Malka G, Lefebvre E and Miquel J L 1997 *Phys. Rev. Lett.* **78** 3314

[14] Wang J X, Ho Y K *et al* 1999 *Phys. Rev.* E **60** 7473

[15] Salamin Y I and Keitel C H 2002 *Phys. Rev. Lett.* **88** 095005
Salamin Y I *et al* 2003 *Phys. Rev.* E **67** 016501

[16] Pang J, Ho Y K, Cao N, Shao L, Xie Y J, Chen Z and Zhang S Y 2003 *Appl. Phys.* B **76** 617

[17] Wang J X *et al.* 1998 *Phys. Rev.* E **58** 6575
Kong Q *et al* 2000 *Phys. Rev.* E **61** 1981

[18] Ho Y K, Wang J X, Feng L, Scheid W and Hora H 1996 *Phys. Lett.* A **220** 189

[19] Wang P X, Ho Y K, Yuan X Q, Komg Q, Cao N, Sessler A M, Esarey E and Nishida Y 2001 *Appl. Phys. Lett.* **78** 2253

[20] Davis L W 1979 *Phys. Rev.* A **19** 1177

[21] Scully M O and Zubairy M S 1991 *Phys. Rev.* A **44** 2656